Supporting Information

High Sensitivity Organic Negative Temperature Coefficient Thermistors Based on Rylene Diimide Derivatives

Meng Zhang[1, 2], Yuanhang Bian[2,4], Meiling Zhang[5], Xujie Dong[2,4], Pengjun Zhao[2], Aimin Chang[2], Can Gao[*3], Yi Liu[*2], Chaoyan Ma[*2], Bolong Zhang[*2]

[1] College of Chemistry and Chemical Engineering, Xinjiang Normal University, Urumqi 830054, China

[2] Key Laboratory of Functional Materials and Devices for Special Environmental Conditions, Chinese Academy of Sciences; Xinjiang Key Laboratory of Electronic Information Materials and Devices; Xinjiang Technical Institute of Physics and Chemistry, Chinese Academy of Sciences, Urumqi 830011, China

[3] Institute of Chemistry, Chinese Academy of Sciences, Beijing 100190, China

[4] Xinjiang Key Laboratory of Solid State Physics and Devices, School of Physics Science and Technology, Xinjiang University, Urumqi 830046, China.

[5] School of Chemistry and Chemical Engineering, Changji University, Changji 831100, China

Corresponding Authors: Bolong Zhang (zhangbl@ms.xjb.ac.cn), Chaoyan Ma (macy@ms.xjb.ac.cn), Yi liu (liu_yi@ms.xjb.ac.cn), Can Gao (cangao@iccas.ac.cn).

Contents

S1. Materials and General Methods

All materials used in were analytically pure. NDI (Naphthalene diimide), PDI (Perylene diimide), and TDI (Terylene diimide) were synthesized as described later. Glass was selected as the substrate material for the thin films. The substrates were first cleaned with ethanol and deionized water. Flash chromatography purification was performed using standard methods on silica gel (Merck Silica Gel 60, 0.036-0.05 mm, 200-300 mesh ASTM). All reactions were monitored by thin-layer chromatography using silica gel (Merck, Silica Gel 60 F254) coated glass sheets, examined under UV lamps (254 nm and 365 nm).

Surface and cross-sectional morphologies of the samples were examined by scanning electron microscopy (SEM) using a Merlin Compact instrument. Fourier-transform infrared (FT-IR) spectra were collected using a PerkinElmer STA8000 spectrometer. X-ray diffraction (XRD) measurements were performed on a Bruker D8 Advance diffractometer. Electrochemical experiments were carried out using a Gamry electrochemical workstation. Thermogravimetric analysis (TGA) was conducted with a NETZSCH STA 449F3 thermal analyzer. Differential scanning calorimetry (DSC) analysis was conducted on a Perkin - Elmer DSC8000 instrument.

S2. Synthesis and characterization of NDI, PDI, and TDI

NDI

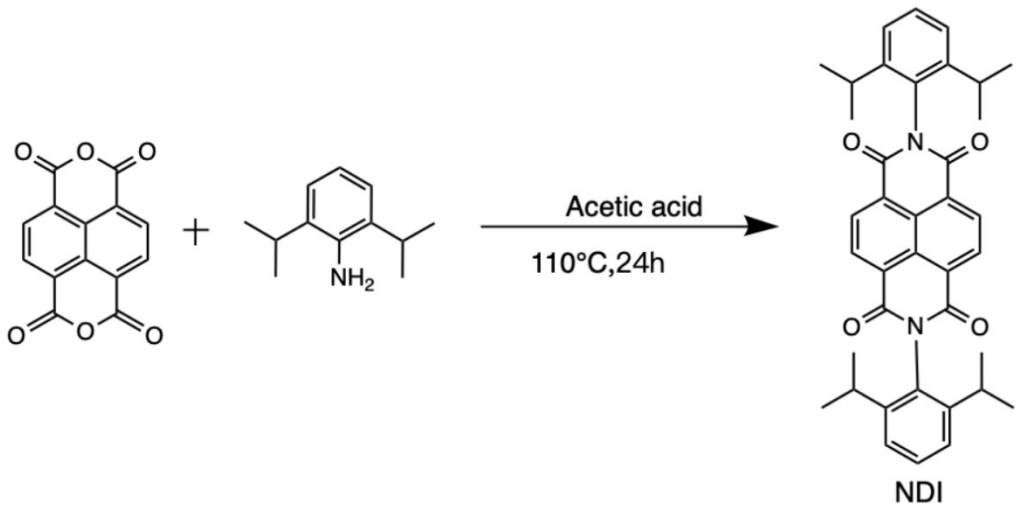

Scheme S1 Synthesis of NDI.

The compound was prepared following the reported literature procedure. [1]

Under a nitrogen atmosphere, Schlenk tube were charged with 1,4,5,8-naphthalenetetracarboxylic dianhydride (1.34 g, 5.0 mmol) and acetic acid (70 mL). The solution was stirred at room temperature and then 2,6-diisopropylaniline (6.32 mL, 5.94 g, 33.5 mmol) was added. The solution was refluxed with 110 ℃ for 24 hours and then cooled to room temperature. The precipitate was washed with anhydrous ethanol (3x25 mL) and filtered the precipitate was dried in vacuum and the crude product

was purified from the residue by rapid column chromatography on silica gel, eluted with DCM. The desired product, a white crystalline powder, was obtained (2.59 g, 4.41 mmol, 88% yield).

^{1}H NMR (400 MHz, $CDCl_3$) δ 8.89 (s, 2H), 7.52 (t, J = 7.8 Hz, 1H), 7.36 (d, J = 7.8 Hz, 2H), 2.71 (p, J = 6.8 Hz, 2H), 1.17 (d, J = 6.9 Hz, 12H).

^{13}C NMR (100MHz, $CDCl_3$) δ 18.89, 24.41, 29.78, 58.94, 77.68, 124.71, 127.37, 130.46, 132.06, 145.99, 163.41.

MS ESI+ (m/z): calcd. for $[M+H^+]$ $C_{38}H_{38}N_2O_4$, 586.731; found $[M+H^+]$, 586.44

FT-IR (cm^{-1}, neat):2928 ,1705 , 1662, 1593, 1361, 1259, 1183, 808, 744

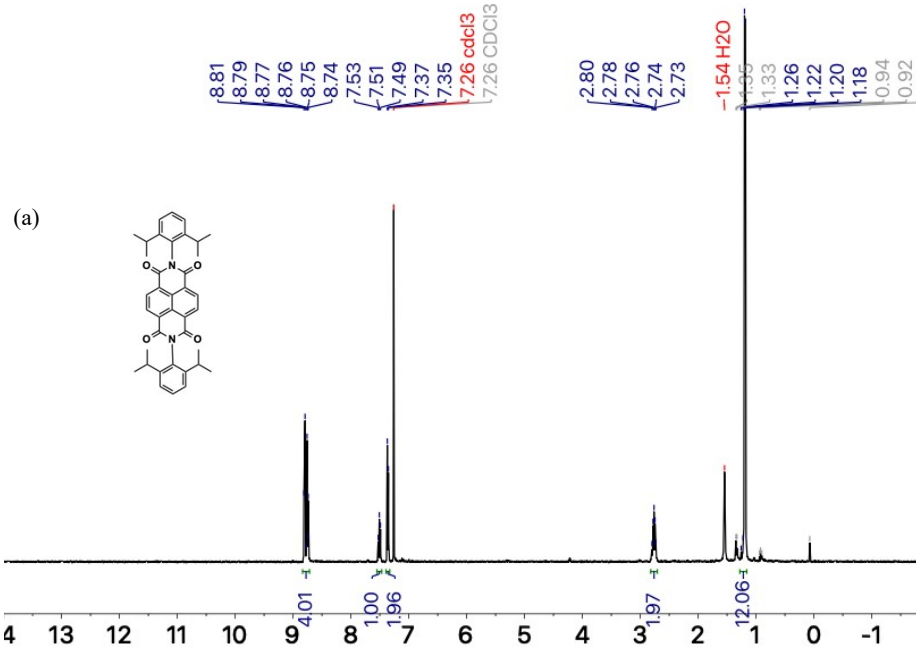

Figure S1 ^{1}H NMR for NDI.

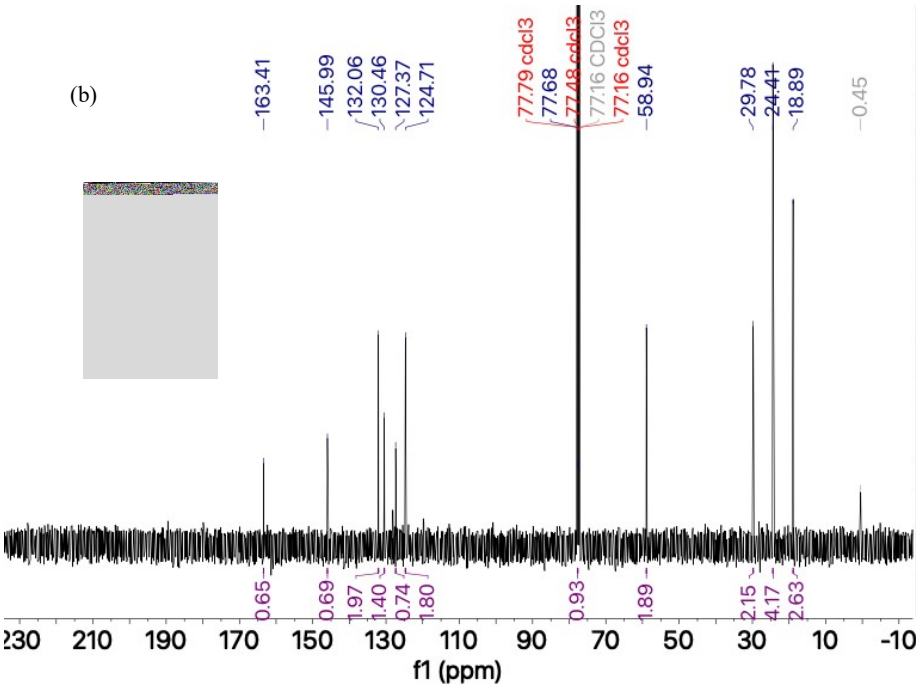

Figure S2 ^{13}C NMR for NDI.

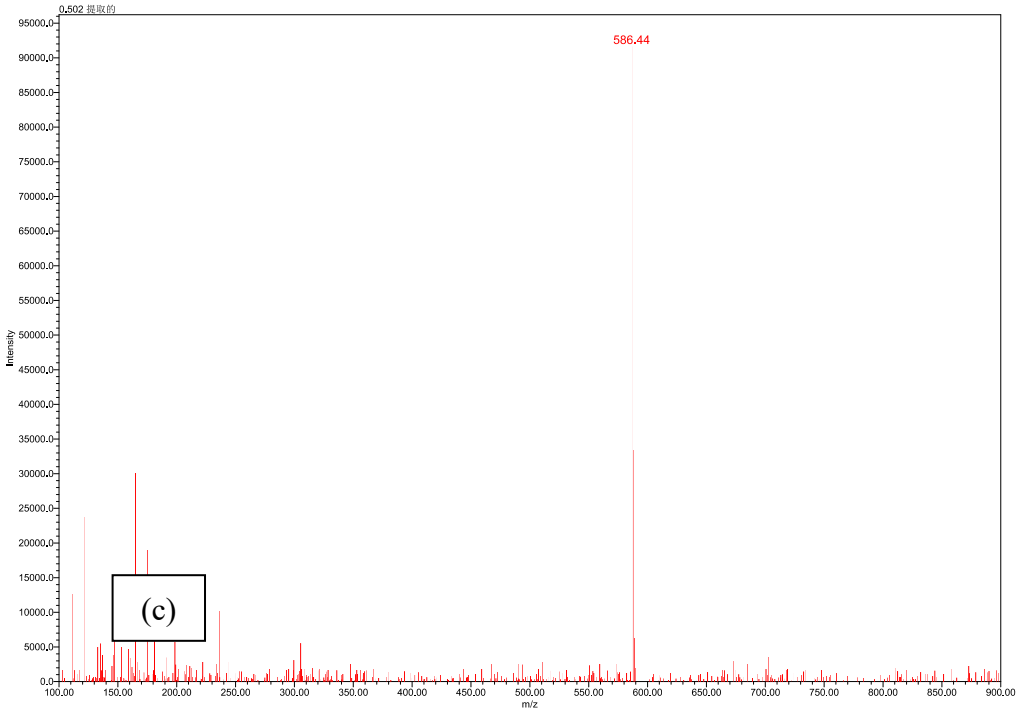

Figure S3 mass spectra for NDI.

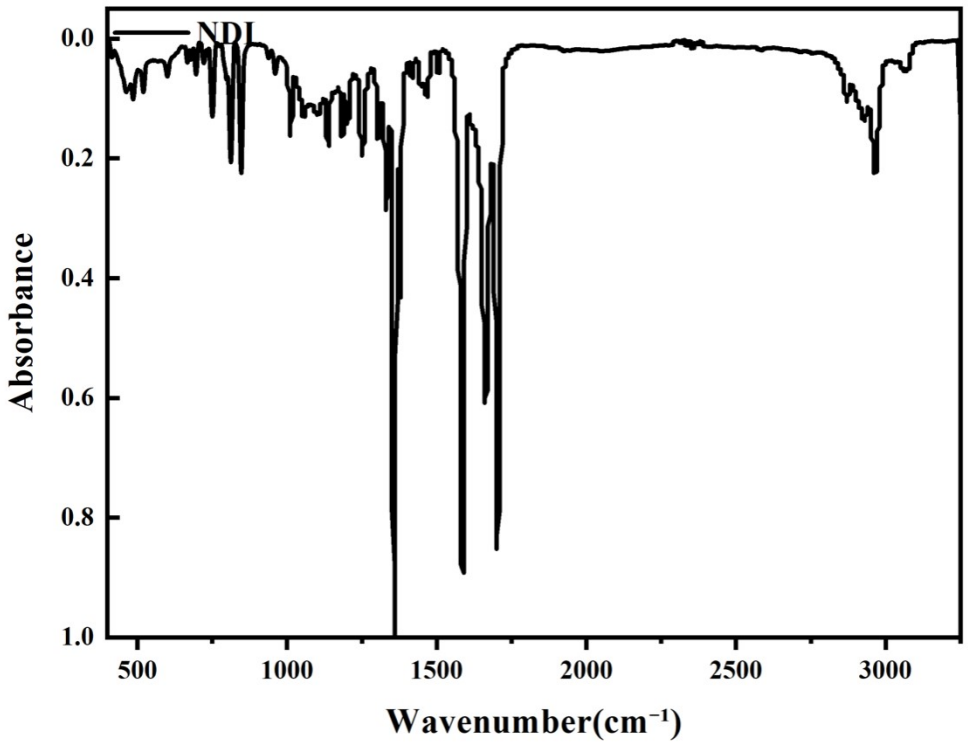

Figure S4 IR for NDI.

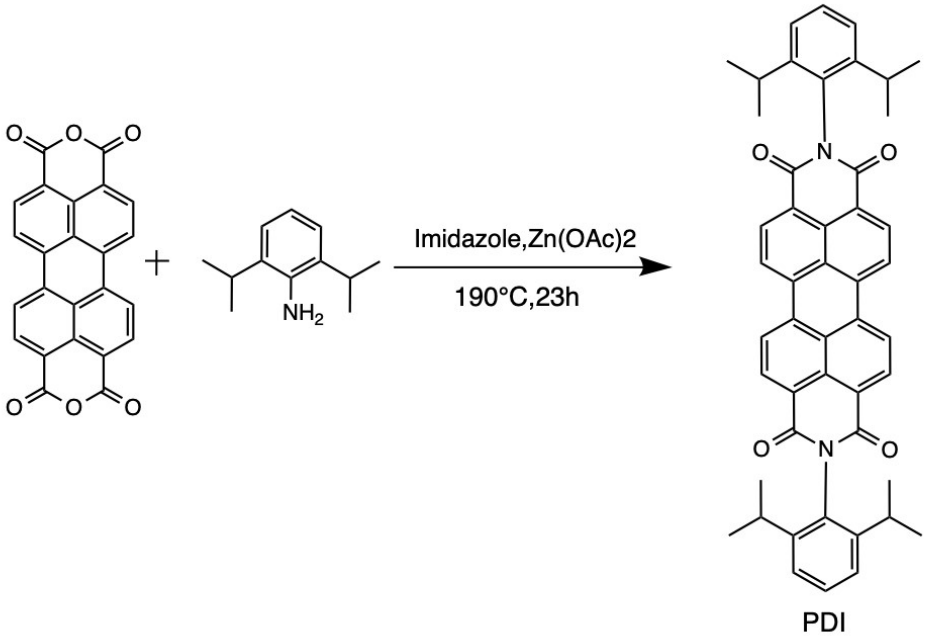

Scheme S2 Synthesis of PDI.

PDI

This Thecompound was synthesized according to literature procedure[2].

In a nitrogen atmosphere, dimethylene dianhydride (PDA) (1g, 0.25 mmol), 2,6-diisopropylaniline (1.82g, 0.57 mmol), imidazole (10.23g, 13.75 mmol), and catalyst Zn $(OAc)_2$(50mg) were added in a Schlenk tube. The reaction mixture was heated to 190℃ and stirred for 18 h. (Multiple syringe needles were inserted to the rubber stopper of the Shlenk tube during the reaction to remove the water vapors). After completion of the reaction, the reaction mixture was cooled to room temperature. The crude product was dissolved in DCM and rinsed, washed with water to remove the imidazole, followed by filtration after removing the residue of water with anhydrous $NaSO_4$. The remaining solvent was removed by rota-evaporator and the residue was then purified by column chromatography on silica gel, eluted with DCM.

The desired compound PDI (77.05 mg, 0.16mmol, 63% yield) was obtained as a red solid.

^{1}H NMR (400 MHz, $CDCl_3$) δ 8.83 – 8.71 (m, 4H), 7.51 (t, *J* = 7.8 Hz, 1H), 7.36 (d, *J* = 7.7 Hz, 2H), 7.26 (s, 3H), 2.76 (p, *J* = 6.9 Hz, 2H), 1.34 (d, *J* = 6.9 Hz, 1H), 1.24 (d, *J* = 16.0 Hz, 1H), 1.19 (d, *J* = 6.9 Hz, 11H).

^{13}C NMR (100 MHz, $CDCl_3$) δ 24.48, 29.70, 77.68, 123.80, 123.90, 124.60, 130.18, 130.99, 132.56, 135.55, 146.11, 163.94.

MS ESI+ (m/z): calcd. for $[M+H^+]$ $C_{48}H_{42}N_2O_4$, 710.872; found $[M+H^+]$, 710.59

FT-IR (cm^{-1}, neat): 2928 ,1705 ,1580 ,1500 ,1360 ,1260 ,1180 ,810 , 740

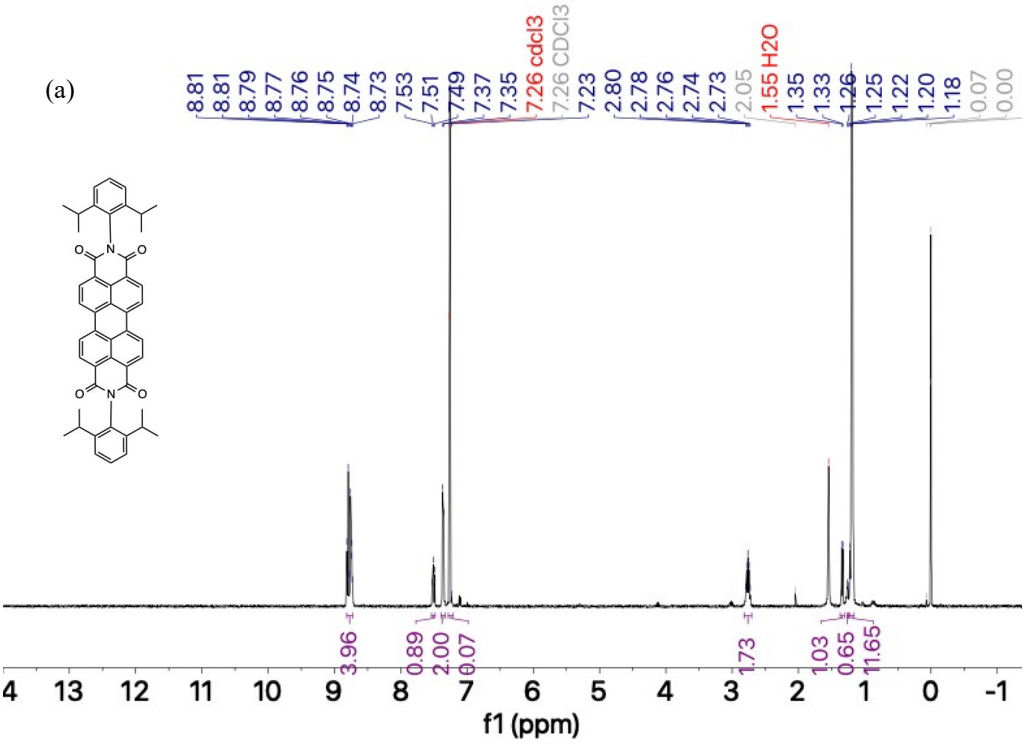

Figure S5 ^{1}H NMR for PDI.

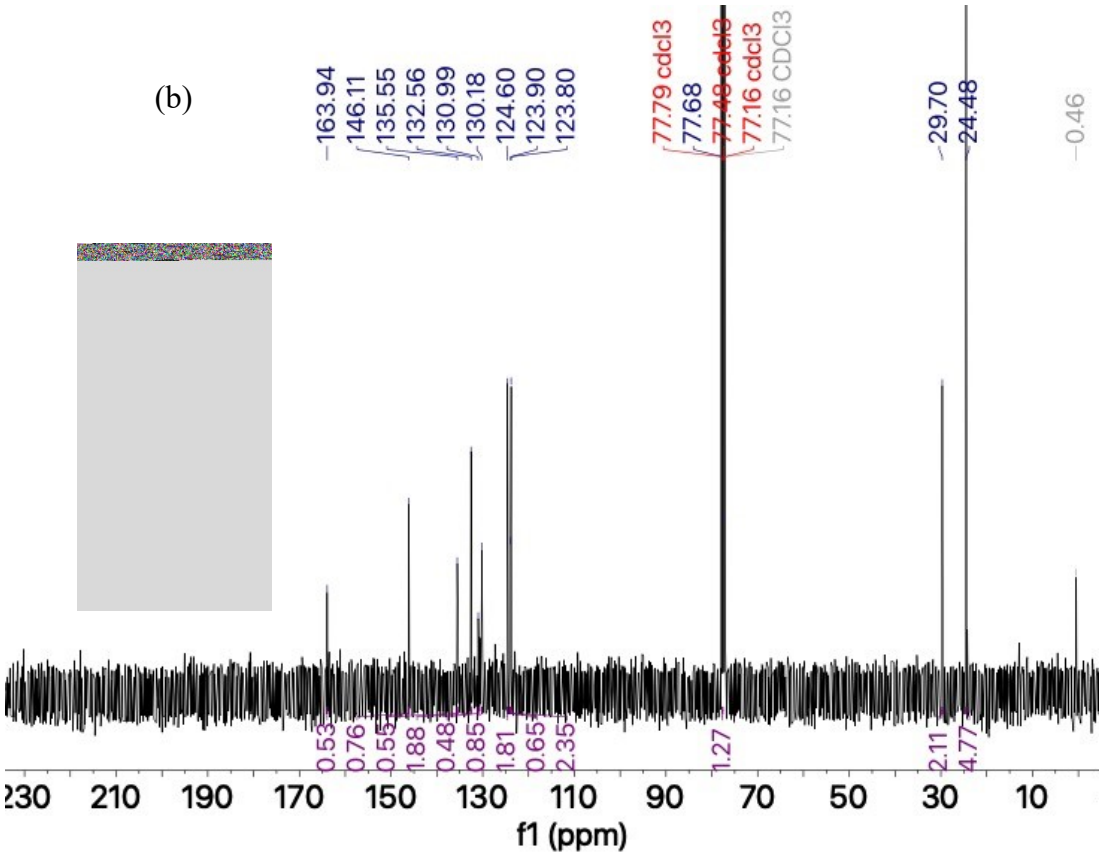

Figure S6 ^{13}C NMR for PDI.

Figure S7 mass spectra for PDI.

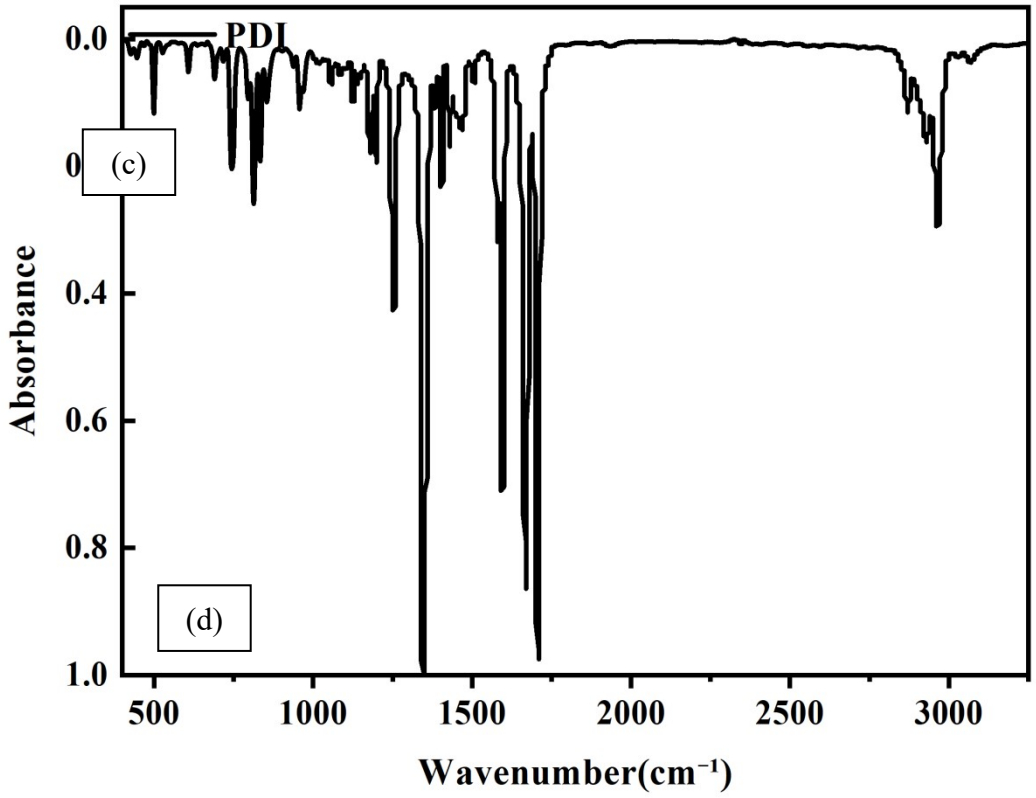

Figure S8 IR for PDI.

TDI

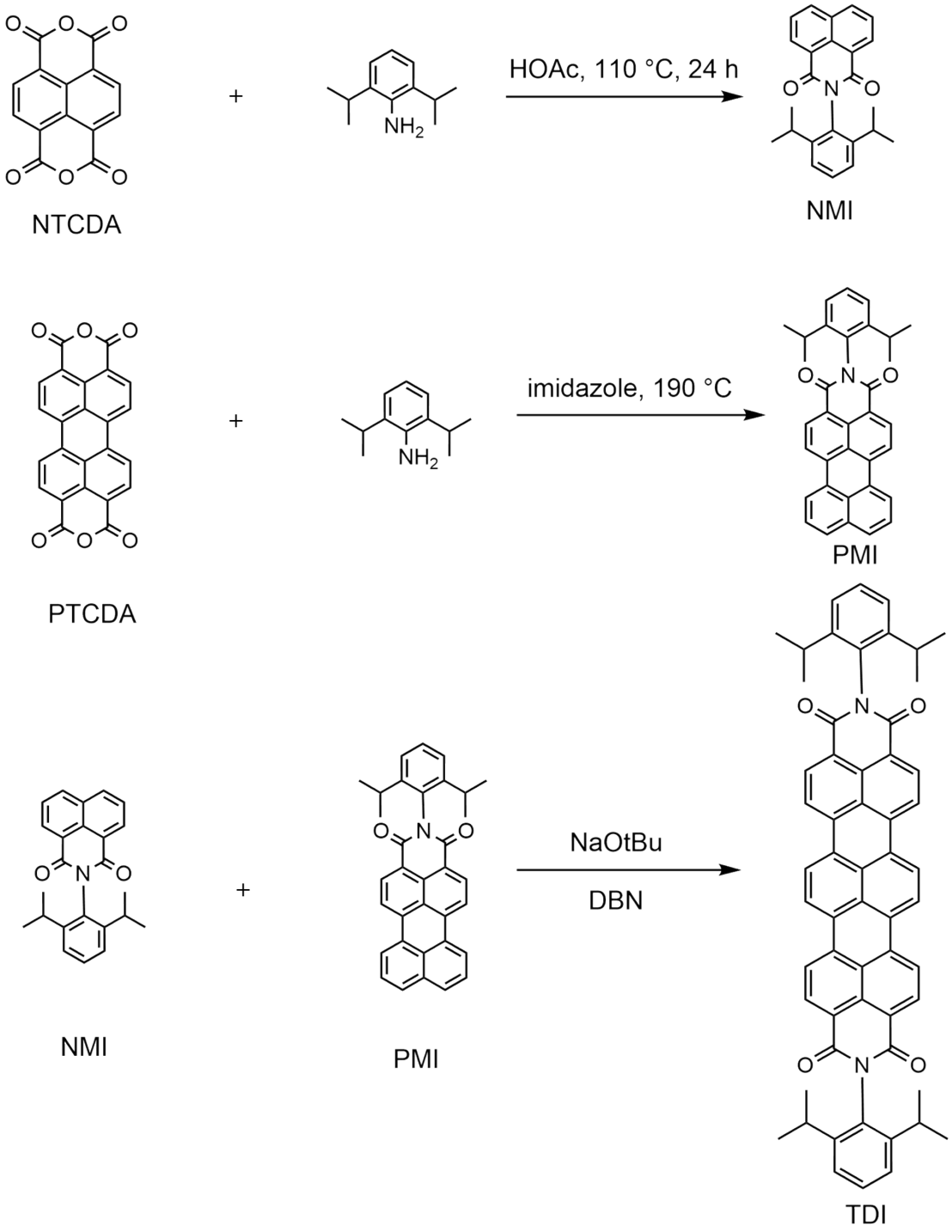

Scheme S3 Synthesis of NMI, PMI, TDI.

Step 1: Preparation of PMI and NMI

NMI:

Under a nitrogen atmosphere, Schlenk tube were charged with NTCDA (5.05 mmol, 1.0 g), glacial acetic acid (20 ml), 2,6-diisopropylaniline (6.06 mmol, 1.2 ml), were heated at 110 °C for 24 h with constant and continuous stirring. The reaction mixture was then cooled to room temperature. Mixture

was diluted with anhydrous ethanol and the precipitate was collected by vacuum filtration. Further purification was carried out by chromatography on a silica gel column, with a solvent mixture of DCM/PET ether (2:1) to afford NMI. The desired compound NMI (1.01 g, 2.82mmol, 56% yield) was obtained as a white solid.

PMI:

PTCDA (9.34 mmol, 3.66 g), 2,6-diisopropylaniline (5.12 mmol, 0.91 g), zinc acetate dihydrate (7.19 mmol, 1.32 g), imidazole (275 mmol, 18.70 g), and H_2O(8ml) were placed in an autoclave. The mixture was heated at 190 °C for 20 hours in the Hydrothermal reactor. The solution was then washed with DCM and the first purification was carried out using a silica gel column short column followed by a silica gel column long column. The desired compound PMI (1.24 g, 2.57mmol, 50.3 % yield) was obtained as a red solid.

TDI：

The compound was prepared following the reported literature procedure[3].

In a dry Schlenk tube, PMI (2.08 mmol, 1 g), NMI (8.32 mmol, 2.96 g) and sodium tert-butoxide (41.58 mmol, 1 g) were added. under a nitrogen atmosphere, Degassing the 1,5-diazabicyclo [4.3.0] non-5-ene (DBN) (41.58 mmol, 5 mL) and diethylene glycol (5 mL) were added to the tube under nitrogen atmosphere. The mixture was stirred vigorously at 130 °C for 23 hours. After cooling to room temperature, the blue mixture was poured into DCM solution and purified using silica gel column chromatography, eluted with DCM. The desired compound TDI (1g, 1.19mmol, 57.3% yield) was obtained as a blue solid.

^{1}H NMR (400 MHz, $CDCl_3$) δ 8.80 – 8.72 (m, 2H), 8.66 (d, J = 8.1 Hz, 1H), 7.36 (d, J = 7.8 Hz, 1H), 7.26 (s, 1H), 2.78 (p, J = 6.8 Hz, 1H), 1.20 (d, J = 6.8 Hz, 6H).

^{13}C NMR (100 MHz, $CDCl_3$) δ 163.60, 145.53, 136.00, 131.90, 124.48, 123.91, 121.43, 77.04, 29.03, 23.86.

FT-IR (cm^{-1}, neat):2928 ,1705 ,1580 ,1500 ,1360 ,1260 ,1180 ,810 , 740

MS ESI+ (m/z): calcd. for [$M+H^+$] $C_{58}H_{46}N_2O_4$, 835.353; found [$M+H^+$], 835.01

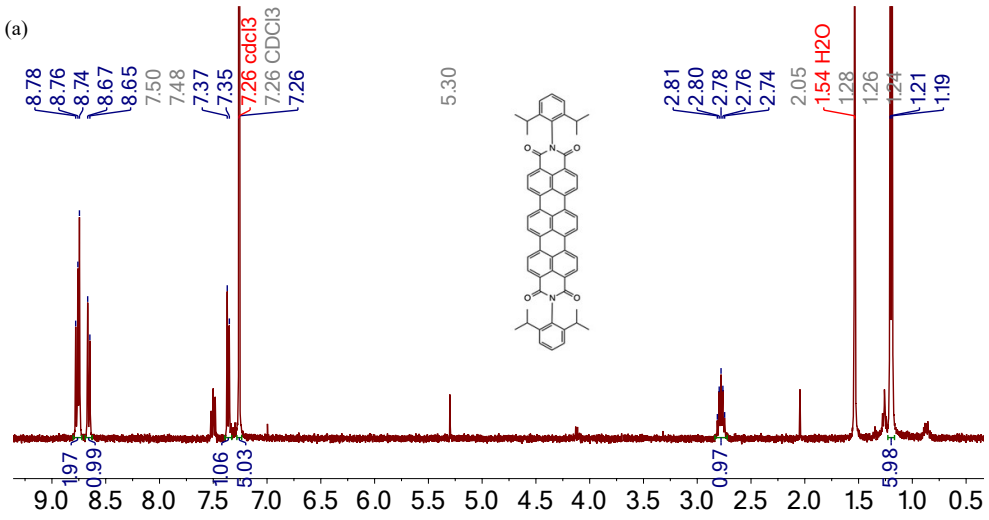

Figure S9 ^{1}H NMR for TDI.

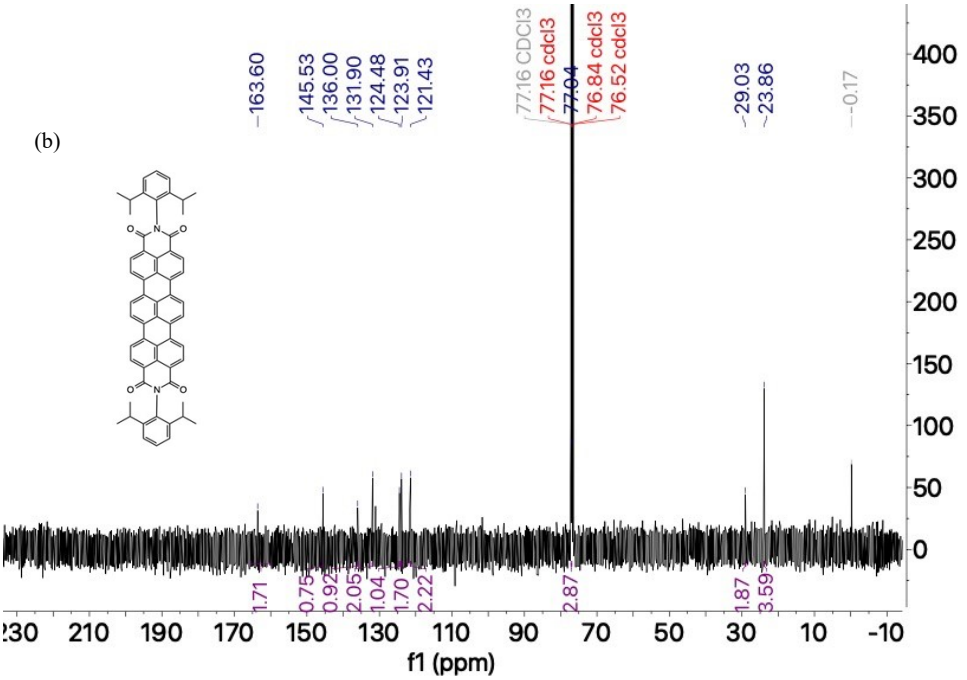

Figure S10 ^{13}C NMR for TDI.

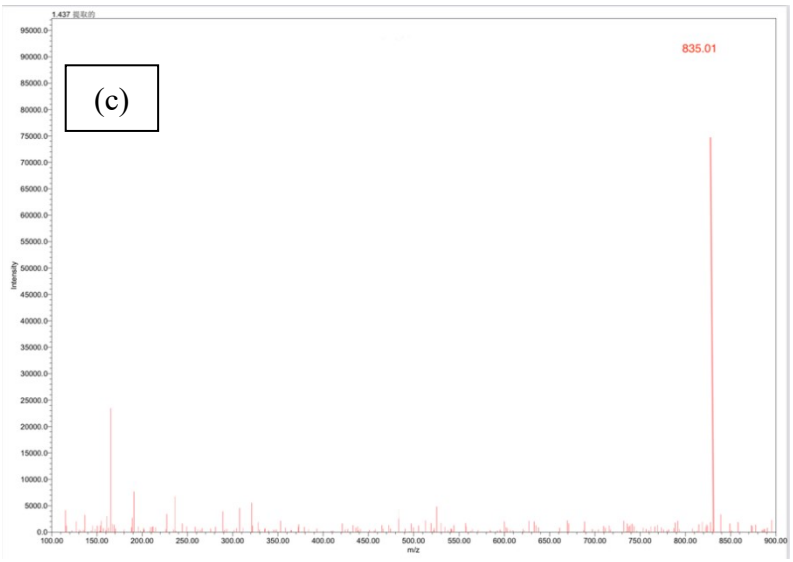

Figure S11 mass spectra for TDI.

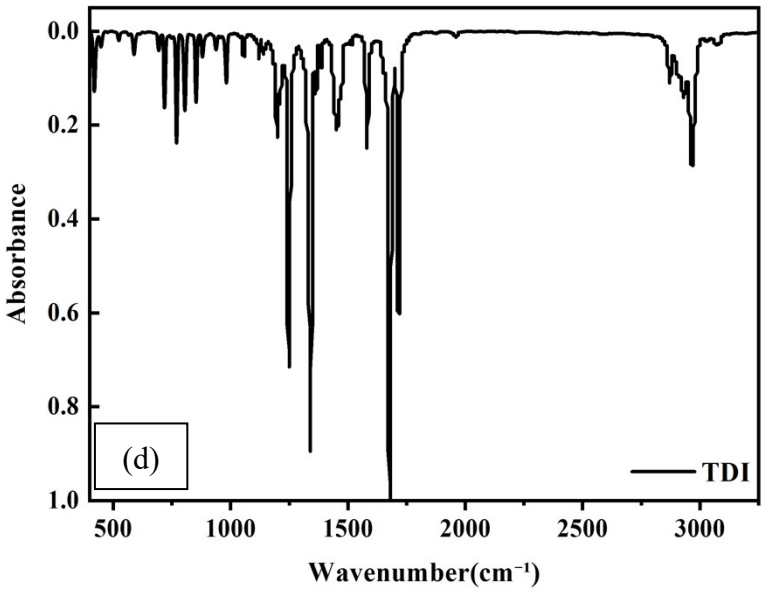

Figure S12 IR for TDI.

S3. X-ray crystal experimental procedures and data of RDIs

NDI[4]

Intensity data for NDI were collected at 180(2) K using Mo Kα radiation (λ = 0.71073 Å). The structure was solved by direct methods (SIR-92) and refined by full-matrix least squares on F^2 using SHELXL-97. Absorption correction: multi-scan; μ(Mo-Kα) = 0.080 mm^{-1}.

Crystal data for NDI ($C_{38}H_{38}N_2O_4$).
M = 586.70, T = 180(2) K, λ = 0.71073 Å; orthorhombic, space group $Pca2_1$.

a = 16.017(1) Å, b = 8.561(1) Å, c = 22.982(1) Å,
α = 90.00°, β = 90.00°, γ = 90.00°.
V = 3151.3(3) Å^3, Z = 4, Dc = 1.237 Mg m^{-3}, F(000) = 1248.
Crystal colour/shape: colourless, block; size 0.46 × 0.23 × 0.10 mm^3.

Data collection and refinement.
Reflections measured = 16,259; independent reflections = 3,661; θmax = 27.48°.
Refinement on F^2; data/restraints/parameters = 3661/1/405; goodness-of-fit on F^2 = 1.101.
Final R indices [I > 2σ(I)]: R1 = 0.0451, wR2 = 0.1196; R indices (all data): R1 = 0.0523, wR2 = 0.1251.

PDI[5]

Intensity data for PDI were collected at 173(2) K using Mo Kα radiation (λ = 0.71073 Å). The structure was solved with SHELXS-97 and refined by full-matrix least squares on F^2 using SHELXL-2014. Molecular graphics were prepared with Bruker SHELXTL. Absorption correction: multi-scan; μ(Mo-Kα) = 0.074 mm^{-1}.

Crystal data for PDI ($C_{48}H_{42}N_2O_4$).
M = 710.83, T = 173(2) K, λ = 0.71073 Å; monoclinic, space group $P2_1/n$.
a = 8.8706(9) Å, b = 19.114(2) Å, c = 12.0638(14) Å,
α = 90.00°, β = 96.149(5)°, γ = 90.00°.
V = 2033.7(4) Å^3, Z = 2, Dc = 1.161 Mg m^{-3}, F(000) = 752.
Crystal colour/shape: red, block; size 0.170 × 0.143 × 0.113 mm^3.

Data collection and refinement.
Reflections measured = 15,372; independent reflections = 3,592; θmax = 25.00°.
Refinement on F^2; data/restraints/parameters = 3592/0/248; goodness-of-fit on F^2 = 0.980.
Final R indices [I > 2σ(I)]: R1 = 0.0766, wR2 = 0.1522; R indices (all data): R1 = 0.2407, wR2 = 0.2279.

TDI

Intensity data for TDI were collected at 170.1 K using Cu Kα radiation (λ = 1.54184 Å). The structure was solved by direct methods and refined by full-matrix least squares on F^2. Thermal ellipsoid plots can be produced with ORTEP-3/WINGX. Absorption correction: multi-scan; μ(Cu-Kα) = 0.630 mm^{-1}.

Crystal data for TDI ($C_{70}H_{58}N_2O_6$).
M = 1023.18, T = 170.1 K, λ = 1.54184 Å; triclinic, space group P-1.
a = 11.6172(5) Å, b = 15.0916(6) Å, c = 16.3539(5) Å,

α = 88.412(3)°, β = 84.937(3)°, γ = 71.019(4)°.

V = 2700.72(19) Å^3, Z = 2, Dc = 1.258 Mg m^{-3}, F(000) = 1080.

Crystal colour/shape: metallic light blue, plate; size 0.30 × 0.25 × 0.20 mm^3.

Data collection and refinement.

Reflections measured = 29,902; independent reflections = 9,787; θmax = 67.999°.

Refinement on F^2; data/restraints/parameters = 9787/0/714; goodness-of-fit on F^2 = 2.670.

Final R indices [I > 2σ(I)]: R1 = 0.1707; wR2 = 0.5282 (all data).

S3.1 Packing analysis of NDI, PDI, and TDI single-crystal structures

Single-crystal analysis further shows that NDI, PDI, and TDI crystallize in the orthorhombic ($Pca2_1$), monoclinic ($P2_1/n$), and triclinic (P-1) systems, respectively. For NDI(CCDC 715666) and PDI(CCDC 1559294), the corresponding crystallographic information was obtained from the reported single-crystal structures [4,5]. Based on these structures, the interplanar distances between adjacent π-conjugated cores are approximately 7 Å for both NDI and PDI (off-centered), whereas no interplanar π-conjugation observed in TDI, indicating distinct intermolecular packing characteristics among the three RDI derivatives.

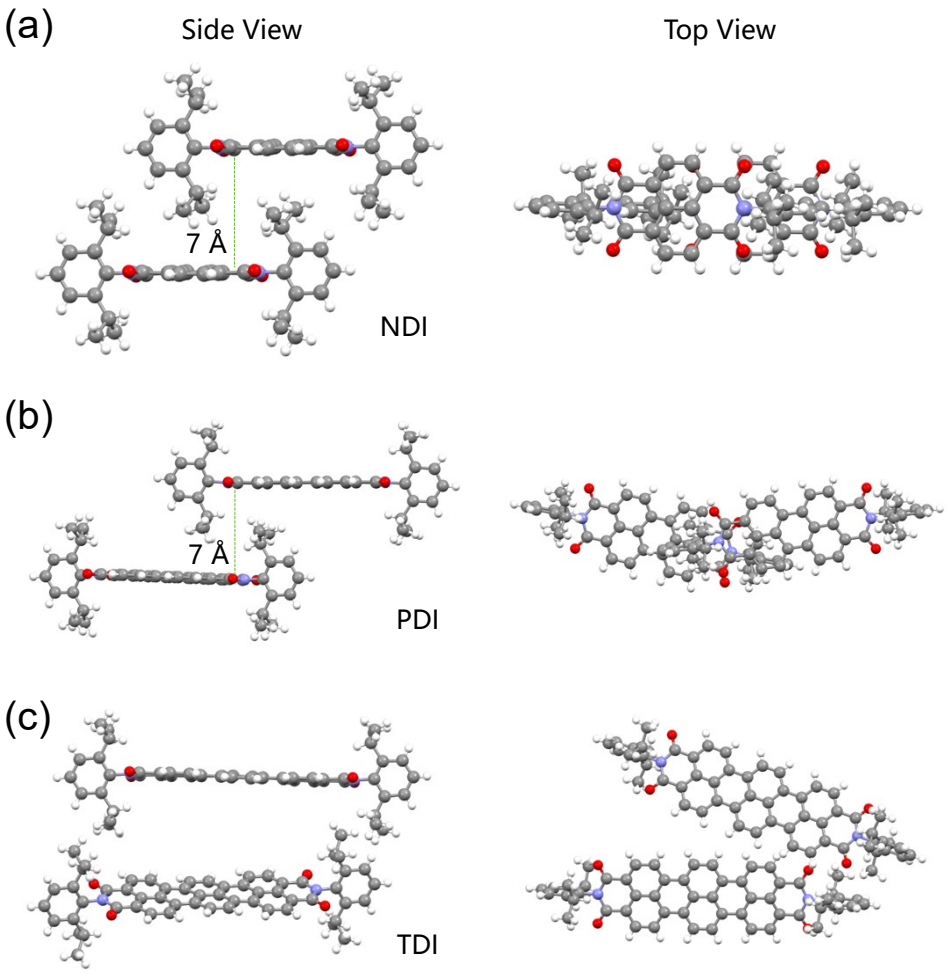

Fig S13 Comparison of the interplanar distances between adjacent π-conjugated cores in the single-crystal structures of NDI, PDI, and TDI.

S4. Electrochemical analysis

All cyclic voltammograms (CV) were acquired in a mixed solution of CH_2Cl_2 and MeCN (9:1 v:v) with 0.1 M $TBAPF_6$. The reference electrode was Ag/Ag+, the working electrode was glassy carbon and platinum was used as the counter electrode. The CVs were acquired at a scan rate of 50 mV/s and ferrocene was used as the internal reference. Therefore, the LUMO and HOMO energy levels of the samples were calculated based on the following equations[6]:

$E_{LUMO} = -(5.1 + E_{red})eV$

$E_{HOMO} = -(5.1 + E_{ox})eV$

Table S1. Summary of the electrochemical properties of the RDIs.

Compound	E_{RED}[a]	E_{LUMO}	E_{OX}[a]	E_{HOMO}	E
	eV	eV	eV	eV	eV
NDI	-0.68	-3.61	1.93	-6.52	2.61
PDI	-0.45	-3.58	1.8	-6.15	2.25

TDI	-0.46	-3.65	1.35	-5.6	1.81

a, vs Fc/Fc+

S5. Thin-film samples preparation

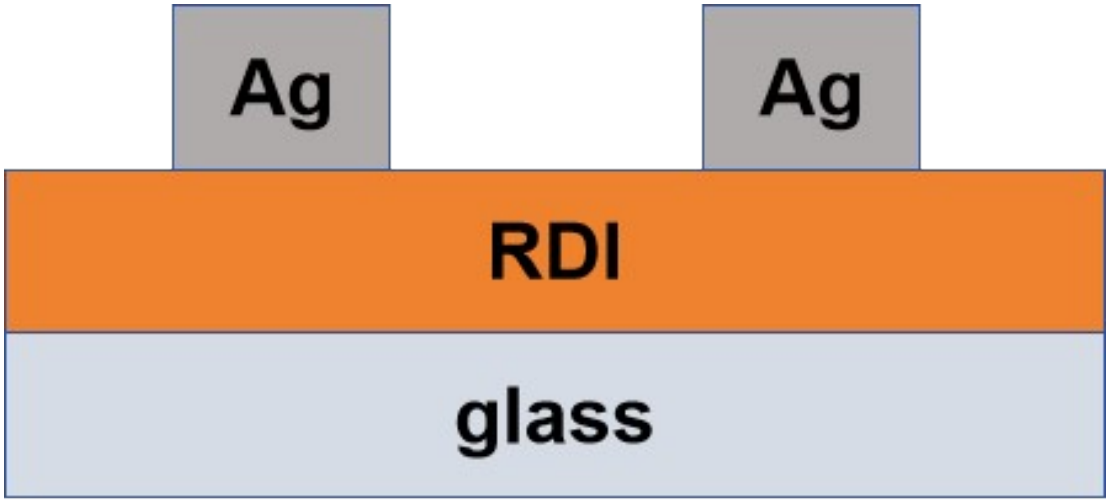

Figure S14 The architecture of RDI devices.

We fabricated three thin-film thermistor devices based on NDI, PDI, and TDI via a shadow-mask process (Figure S14), with organic film resistors prepared through solution processing. Glass substrates were cut into 1 cm × 1 cm pieces, followed by sequential ultrasonic cleaning in ethanol and deionized water for 20 min each, dried under a high-purity nitrogen stream, and finally subjected to 10 min plasma treatment.

The organic thermistor films were first prepared on the cleaned glass substrates by spin coating. During spin coating, a fixed volume of 10 mg mL^{-1} RDI solution in chlorobenzene was dispensed onto the substrate surface until complete coverage was achieved, followed by bubble removal. Spin-coating parameters were set at 500–3000 rpm with an acceleration rate of ~1000 rpm s^{-1} for 30 s to form uniform films. Post-coating thermal annealing at 100 °C for 5 min was conducted to remove residual solvent.

After film formation, silver electrodes (200 nm) were deposited by vacuum deposition through a shadow mask to define conductive channels with a length of 200 μm and a width of 20 μm. Finally, the thermistor devices underwent thermal annealing at 200 °C in ambient atmosphere for 10 min to enhance crystallinity and interfacial properties.

S6. Scanning electron microscopy (SEM)

To further quantify the morphology evolution induced by thermal annealing, the grain/domain sizes in the SEM images were statistically analyzed using ImageJ, and the corresponding results are

shown in Figure S15. Specifically, Figures S15a–c show the SEM images of NDI, PDI, and TDI thin films before annealing, respectively, while Figures S15d–f show the corresponding films after annealing. The average grain size (AGS) of the NDI film increased from 1.69 μm before annealing to 2.47 μm after annealing. For PDI, the AGS increased from 2.29 μm to 2.84 μm, while for TDI it increased from 0.33 μm to 0.87 μm after annealing. These results further confirm that thermal annealing promotes grain/domain growth and structural reorganization in all three RDI thin films.

Cross-sectional SEM images comparing NDI, PDI and TDI thin films before and after annealing.The pristine films (a–c) exhibit uniform thicknesses of approximately 115 nm (NDI), 150 nm (PDI), and 125 nm (TDI), respectively. After thermal annealing (d–f), the film thickness increases to around 190 nm, 165 nm, and 189 nm, respectively, accompanied by distinct morphological changes. In particular, the NDI film shows crack formation, while the PDI and TDI films display rougher surfaces and interfacial undulations. These observations suggest thermal expansion and structural rearrangement upon annealing, with varied responses depending on the chemical structure of the materials.

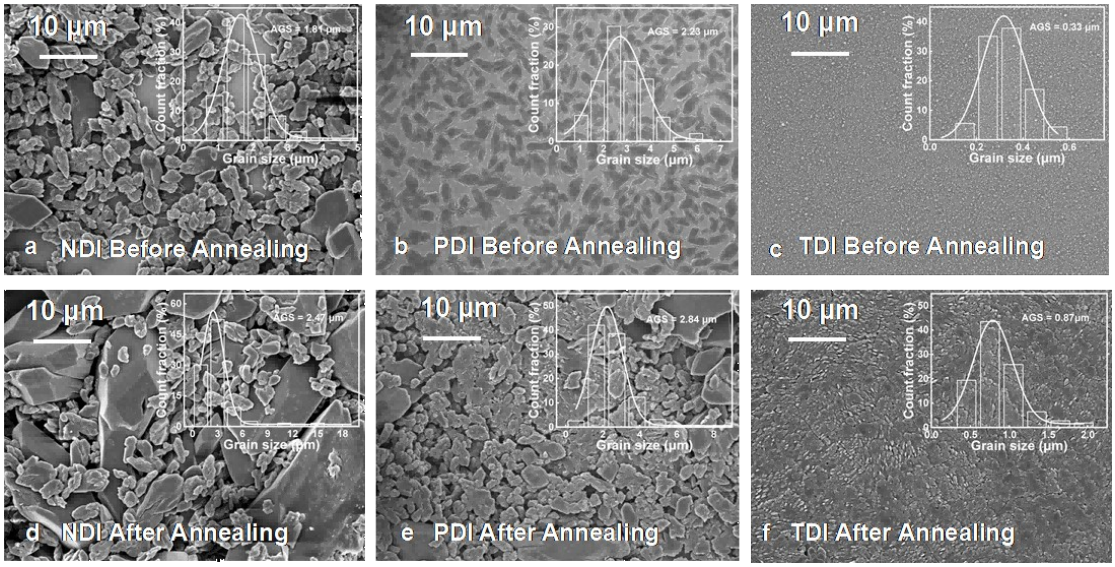

Figure S15 SEM images of the RDI thin films before and after annealing, together with the corresponding grain-size distributions obtained from ImageJ analysis: (a) NDI before annealing, (b) PDI before annealing, (c) TDI before annealing, (d) NDI after annealing, (e) PDI after annealing, and (f) TDI after annealing. The average grain sizes (AGS) are approximately 1.69 μm and 2.47 μm for NDI before and after annealing, 2.29 μm and 2.84 μm for PDI before and after annealing, and 0.33 μm and 0.87 μm for TDI before and after annealing.

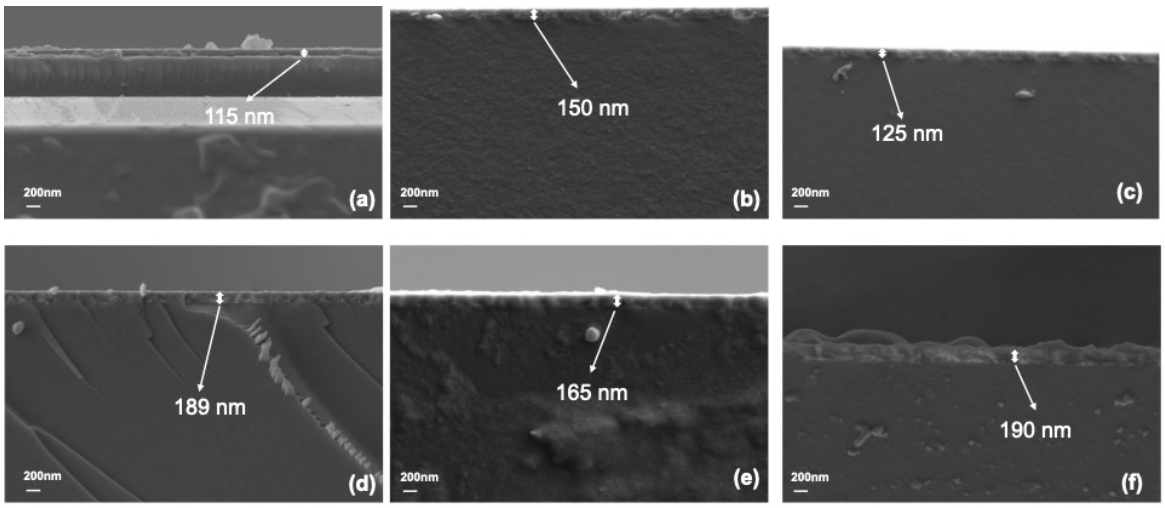

Figure S16 Cross-sectional SEM images of NDI, PDI, and TDI thin films. Scale bars: 200 nm. Representative film thicknesses: (a) 115 nm, (b) 150 nm, (c) 125 nm, (d) 189 nm, (e) 165 nm, and (f) 190 nm. Imaging conditions: EHT = 5.0 kV, working distance = 6.3 mm, detector = SE2.

S7. Temperature-dependent resistance (R-T) measurements

R–T measurements were carried out under vacuum conditions (1.5×10^0 Pa) using a cryogenic probe station (PSM-LN2-2H, Shanghai Yinqi Refrigeration Equipment Co., Ltd.) coupled with a semiconductor analyzer (FS-Pro, Primarius). Temperature-dependent electrical measurements were carried out on approximately 150 independently fabricated devices in total, including around 50 devices for each material system. Each device was measured three times, and representative results are presented in the main text.

S8. Calculation of TCR Values Summarized in Table 2

To allow a quantitative comparison between our rylene diimide (RDI) thermistors and previously reported printed and organic NTC thermistors, the temperature coefficients of resistance (TCRs) listed in Table 2 of the main text were either taken directly from the literature or calculated from the reported thermistor constant B, activation energy Ea , or empirical current–temperature relations in Refs.

For NTC thermistors following an Arrhenius-type behaviour, the resistance is expressed as

$$R(T) = R_0 exp\left(\frac{B}{T}\right) = R_0 exp\left(\frac{E_a}{k_B T}\right),$$

where R_0 is a pre-exponential factor, B is the thermistor constant and Ea is the activation energy. The (instantaneous) TCR at temperature T is defined as

$$TCR(T) = \frac{1}{R}\frac{dR}{dT} = -\frac{B}{T^2}.$$

In Table 2, we report the magnitude of the TCR in units of % K^{-1}:

$$TCR_{\%}(T) = -\frac{B}{T^2} \times 100\%. \quad \text{(S1)}$$

When only the activation energy is reported, the corresponding thermistor constant is obtained from

$$B = \frac{E_a}{k_B}, \quad \text{(S2)}$$

and inserted into Eq. (S1) at a representative temperature (typically 298–300 K or at the centre of the working temperature window) to obtain the TCR value quoted in Table 2.

In some reports, such as the P3HT-coated elastic carbon foam temperature sensor[6], the authors directly provide the sensitivity

$$S = \frac{\Delta R}{R_0 \Delta T}$$

in units of % K^{-1}. In these cases, the reported sensitivity is equivalent to the average TCR within the corresponding temperature interval and is used directly in Table 2.

Table S2 summarises how the TCR values for representative materials were obtained.

Material / device	Literature data used	Method to obtain TCR	TCR used in Table 2
P3HT-NF / SEBS rubbery thermistor[7]	Reported TCR = −7.73 to −6.75 % K^{-1} in 24–45 °C range	Directly taken from Ref. [5]	−6.8 % K^{-1} (24–45 °C)
P3HT-coated elastic carbon foam[8]	Reported sensitivity S = 1.81 % K^{-1} in 30–60 °C range	S treated as average TCR	−1.81 % K^{-1} (30–60 °C)
PANI/Mn_3O_4 composite[9]	Thermistor constants B = 3625 K and 3745 K (20–110 °C and 20–160 °C)[7]	Eq. (S1) with (T = 300) K gives TCR(300 K) ≈ −4.0 to −4.2 % K^{-1}	−4.0 % K^{-1} (≈25–150 °C)
POMANI–Mn_3O_4 thin film[10]	Thermistor constant B = 8080 K in the 100–170 °C range[8]	Eq. (S1) with T = 400 K gives TCR(400 K) ≈ −5.0 % K^{-1}	−5.0 % K^{-1} (100–170 °C)
PPy/$(PhSe)_2$	Temperature coefficient α_t(300 K) =	Directly adopted as TCR	−0.91 % K^{-1}

Material / device	Literature data used	Method to obtain TCR	TCR used in Table 2
nanocomposite[11]	-0.91 % K^{-1} listed in Table 1 [9]	at 300 K	(30–80 °C, NTC region)
Pentacene/AgNP thermistor and pentacene thermistor[12]	Activation energies Ea = 0.361 eV (AgNP/pentacene) and 0.157 eV (pentacene) extracted from Arrhenius plots[10]	TCR ≈ −4.72 and −2.05 % K^{-1}	−4.72 / −2.05 % K^{-1} (20–50 °C)
CuPc/PTCDI pn diode[13]	Temperature-dependent drain current $I_d(T)$ described by a linear relation in the 20–100 °C range[11]	$R = V/I_d(T)$; TCR = $-(1/I_d)\, dI_d/dT$ evaluated at mid-range (T) gives TCR ≈ −1.3 % K^{-1}	−1.3 % K^{-1} (20–100 °C)
BN-, BPE- and DD-PTCDI nanofiber thermistors[14]	Dark-state activation energies Ea = 0.628, 0.465 and 0.169 eV in the 25–80 °C range[12]	(B = E_a/k_{\rm B}) and Eq. (S1) at 298 K give TCR ≈ −8.21, −6.08 and −2.21 % K^{-1}	−8.21 / −6.08 / −2.21 % K^{-1} (25–80 °C)
NDI-based donor–acceptor coordination polymer[15]	Thermistor constant (B = 4671) K and reported TCR ≈ 0.72 % K^{-1} (40–220 °C)[13]	Reported value used directly as average TCR	−0.72 % K^{-1} (≈40–220 °C)

For other printed thermistors based on graphene inks, reduced graphene oxides, PEDOT:PSS and NiO/CBNP composites, the TCR values were taken directly from the original references, where they are explicitly reported as % K^{-1} within the indicated temperature ranges.

S9. Theoretical calculation

All quantum-chemical calculations were performed with Gaussian 16 (G16).[16] Geometries were optimized in solution using density functional theory (DFT) at the B3LYP/6-31G(d,p) level with the polarizable continuum model (PCM, IEFPCM) for toluene (scrf=(solvent=toluene)). Each optimized structure was characterized by a harmonic frequency calculation at the same level (opt freq) to verify the nature of the stationary point (no imaginary frequencies) and to obtain thermal corrections. Unless otherwise stated, thermochemical quantities were evaluated under Gaussian defaults (298.15 K, 1 atm). Solution-phase Gibbs free energies were obtained by adding the PCM electronic energy of the optimized structure to the thermal correction from the frequency analysis at the same level.

NDI

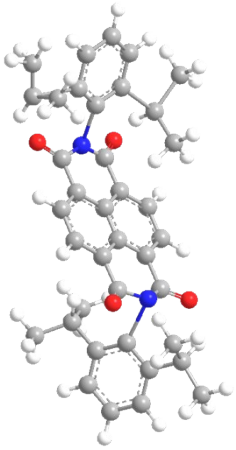

Figure S17 Optimized geometry of NDI at the B3LYP/6-31G(d) level.

Table S3. Cartesian coordinates (Å) of the optimized structure for the NDI calculated at the B3LYP/6-31G (d) level.

Atom	X (Å)	Y (Å)	Z (Å)	Atom	X (Å)	Y (Å)	Z (Å)
C	-0.73552	-0.3479	-2.27325	C	-4.65563	2.412242	-0.1102
C	0.601209	-0.33278	-2.28525	H	-7.29372	2.038261	-0.07043
C	1.293073	-0.16242	-1.14616	H	-8.53914	-0.02585	0.054354
C	0.629421	-0.00471	0.019559	H	-7.38962	-2.13612	0.175994
C	-0.72957	-0.02106	0.03181	H	-3.90898	-2.77039	-1.77789
C	-1.41043	-0.19417	-1.12168	C	6.643173	1.210227	-0.14665
H	-1.24035	-0.49312	-3.24313	C	5.298249	1.21945	-0.13691
H	1.091859	-0.46568	-3.26401	C	4.614501	-2.47307	0.235929
C	-2.75414	0.131239	1.257667	H	7.25414	-2.02248	0.166926
C	1.309866	0.170045	1.17317	H	8.431347	0.075505	-0.04934
C	-1.3935	0.142781	1.196389	H	7.209617	2.150018	-0.24451
N	-3.40234	-0.092	0.060699	C	4.560707	2.548569	-0.26695
C	-2.77173	-0.21684	-1.15832	H	-3.31608	-3.95218	1.178526
C	2.653648	-0.15258	-1.20778	H	-3.61686	-2.41618	2.04086
C	0.634738	0.331201	2.323492	H	-2.64533	-2.45947	0.506067
N	3.300131	0.024924	-0.00403	H	-3.54868	2.262993	-0.09084
C	2.671274	0.189753	1.210753	C	-4.97638	3.332089	1.080174
C	-0.70212	0.318705	2.334853	C	-4.95504	3.103418	-1.45176
H	-1.19279	0.455	3.313075	H	-4.35735	4.037027	-1.56352
O	-3.42528	-0.3312	-2.17322	H	-4.69765	2.437517	-2.30753
H	1.139514	0.478151	3.293013	H	-6.02624	3.387258	-1.55067
O	-3.39341	0.290596	2.275738	H	-4.37164	4.266834	1.037115
O	3.294192	-0.28602	-2.22857	H	-4.74405	2.828626	2.046585
O	3.326612	0.338593	2.219973	H	-6.04599	3.637095	1.103339

C	-4.83145	-2.68432	0.22271	H	3.505284	-2.33617	0.231811
H	-5.57234	-3.32474	0.771214	C	4.950945	-3.13854	1.58104
C	-4.75523	-0.11403	0.072338	C	4.932373	-3.40087	-0.94852
C	-5.39294	1.077744	-0.00464	H	4.351963	-4.34949	-0.88047
C	-6.73751	1.089711	-0.00473	H	4.667248	-2.91558	-1.91601
C	-7.43642	-0.04866	0.063226	H	6.009076	-3.67803	-0.98959
C	4.653339	0.038511	-0.01594	H	4.371875	-4.08057	1.717255
C	5.323375	-1.12958	0.093283	H	4.698043	-2.46424	2.431569
C	6.667719	-1.09396	0.079343	H	6.028787	-3.40213	1.662769
C	7.328423	0.064769	-0.03954	H	3.454539	2.38989	-0.24298
C	-3.53593	-2.87007	1.027418	C	4.860052	3.219925	-1.61791
C	-4.68656	-3.29472	-1.18153	C	4.881232	3.483008	0.91164
H	-4.38738	-4.36645	-1.12637	H	4.28094	4.419811	0.853993
H	-5.64354	-3.24612	-1.74962	H	4.64338	2.992864	1.883642
C	-6.78416	-1.21503	0.132429	H	5.952845	3.781627	0.933214
C	-5.43817	-1.28056	0.144445	H	5.930958	3.504193	-1.71897

PDI

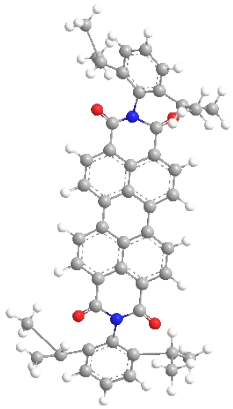

Figure S18 Optimized geometry of PDI at the B3LYP/6-31G(d) level.

Table S4. Cartesian coordinates (Å) of the optimized structure for the PDI calculated at the B3LYP/6-31G (d) level.

Atom	X (Å)	Y (Å)	Z (Å)	Atom	X (Å)	Y (Å)	Z (Å)
C	-0.73506	0.013603	-1.249816	C	7.412091	3.312906	-1.440111
C	0.735073	-0.01356	-1.249808	H	0.97984	-0.075957	-3.391118
C	1.432019	2.1e-05	6e-06	H	3.437046	-0.093508	-3.349553
C	0.73506	0.013601	1.249813	H	-0.97984	-0.075962	3.391115
C	-0.735074	-0.01356	1.249806	H	-3.437011	0.093542	-3.34959
C	-1.432019	2.2e-05	-9.00E-06	H	-0.979805	0.075994	-3.391128
C	-2.861486	2e-05	-1.60E-05	H	-3.437046	-0.093517	3.349551
C	1.479181	-0.051336	-2.430783	H	3.43701	0.09353	3.349588

C	2.877535	-0.063092	-2.421448	H	0.979804	0.075988	3.391126
C	3.572789	-0.033406	-1.224353	H	9.785276	-2.138445	0.108119
C	-1.479181	-0.051338	2.430781	H	11.016328	-4.70E-05	5.4e-05
C	-3.572777	0.033442	-1.224391	H	9.785323	2.138376	-0.108024
C	-2.87751	0.063128	-2.421478	H	-9.785268	-2.138454	-0.108152
C	-1.479155	0.051375	-2.430799	H	-11.016328	-6.30E-05	-4.10E-05
C	-2.877535	-0.063096	2.421445	H	6.028557	-2.367262	0.118725
C	-3.57279	-0.033409	1.224351	H	6.028612	2.367282	-0.118655
C	-5.054361	-0.040911	1.246433	H	-9.785331	2.138363	0.108075
N	-5.705354	1e-05	-3.10E-05	H	-6.028548	-2.367253	-0.118781
C	-5.054348	0.040938	-1.246489	H	-6.028621	2.367284	0.118696
C	2.861486	1.7e-05	1.4e-05	H	-7.152136	2.908014	-2.02864
C	3.572776	0.033434	1.224389	H	-8.470809	3.704486	-1.155821
C	5.054361	-0.040897	-1.246436	H	-6.833662	4.367725	-1.070132
C	2.87751	0.06312	2.421476	H	-8.472831	3.575809	1.512902
C	1.479155	0.05137	2.430796	H	-7.156847	2.696403	2.307118
N	5.705354	7e-06	2.9e-05	H	-6.83497	4.242289	1.495894
C	5.054348	0.040916	1.246488	H	-7.152002	-2.908012	2.028571
C	-7.158299	-7.00E-06	-3.80E-05	H	-6.83351	-4.367719	1.070066
C	7.158299	-6.00E-06	3.7e-05	H	-8.470673	-3.704525	1.155784
C	7.83477	-1.231137	0.061838	H	-7.156785	-2.696432	-2.307187
C	9.234417	-1.203885	0.060921	H	-8.472734	-3.575871	-1.51295
C	9.930116	-3.60E-05	4.9e-05	H	-6.834851	-4.2423	-1.495953
C	9.234443	1.203828	-0.060831	H	7.152035	-2.90797	-2.02863
C	7.834797	1.231112	-0.06176	H	8.470699	-3.704495	-1.155847
O	-5.698047	-0.07875	2.286652	H	6.833539	-4.367699	-1.070158
O	-5.698022	0.078753	-2.286717	H	6.83486	-4.242332	1.495865
O	5.698046	-0.078751	-2.286655	H	7.156779	-2.696478	2.307132
O	5.698022	0.078754	2.286714	H	8.472739	-3.575895	1.512888
C	-7.834766	-1.231139	-0.061859	H	7.152111	2.907971	2.028698
C	-9.234413	-1.203892	-0.060938	H	8.470788	3.704465	1.155905
C	-9.930116	-4.70E-05	-4.00E-05	H	6.83364	4.367702	1.07022
C	7.103774	-2.567443	0.127931	H	7.156847	2.696454	-2.307064
C	7.103834	2.567435	-0.127861	H	8.472824	3.575847	-1.512822
C	-9.234448	1.203818	0.060862	H	6.83496	4.242321	-1.495807
C	-7.834802	1.231107	0.061786	C	-7.409825	-3.43683	1.106228
C	-7.103763	-2.56744	-0.127983	C	-7.412007	-3.312902	-1.440242

C	-7.103844	2.567432	0.127912	C	7.40985	-3.436806	-1.106296
C	-7.409953	3.43682	-1.106288	C	7.412011	-3.31293	1.440177
C	-7.412097	3.312873	1.44018	C	7.409933	3.436798	1.10636

TDI

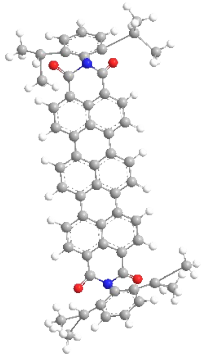

Figure S19 Optimized geometry of TDI at the B3LYP/6-31G(d) level.

Table S5. Cartesian coordinates (Å) of the optimized structure for the TDI calculated at the B3LYP/6-31G (d) level.

Atom	X (Å)	Y (Å)	Z (Å)	Atom	X (Å)	Y (Å)	Z (Å)
C	-5.05002	-0.22404	-2.41667	C	10.02137	1.22669	-0.13556
C	-3.65077	-0.22556	-2.42496	O	7.879722	-0.23106	-2.29991
C	-2.90361	-0.1164	-1.24309	O	7.879761	0.231084	2.299824
C	-3.60589	0.000115	2.21E-05	C	9.285416	-2.55703	0.284624
C	-5.03819	0.000103	2.96E-05	C	9.603689	-3.51261	-0.8885
C	-5.75046	-0.11315	-1.22193	C	9.583737	-3.21373	1.652472
C	-2.90359	0.116632	1.243126	C	9.286004	2.556947	-0.2846
C	-3.65075	0.225777	2.42501	C	9.584541	3.213648	-1.65239
C	-5.04999	0.224232	2.416728	C	9.604474	3.512364	0.888601
C	-5.75045	0.113328	1.221994	H	-5.61111	-0.30932	-3.34
C	-1.43525	-0.1178	-1.23811	H	-3.15212	-0.31424	-3.38113
C	-0.72061	0.000121	6.12E-06	H	-3.15209	0.314458	3.381176
C	-1.43524	0.118043	1.238132	H	-5.61107	0.309479	3.340068
C	0.720653	0.00012	-2.5E-06	H	1.200327	0.325985	3.372152
C	1.435296	0.12082	1.237844	H	-1.20024	0.323378	3.372428
C	0.696685	0.233868	2.418815	H	-1.20028	-0.32316	-3.37241
C	-0.69661	0.232202	2.418988	H	1.200287	-0.32577	-3.37216
C	-0.69664	-0.23197	-2.41897	H	-11.9741	2.140188	-0.13091
C	0.696656	-0.23364	-2.41882	H	-13.2072	-0.00035	-0.00012
C	1.435281	-0.12059	-1.23786	H	-11.9738	-2.14071	0.130745
C	-7.22517	0.114975	1.241699	H	-8.20965	-2.36282	0.166015

N	-7.88361	3.9E-05	5.19E-05	H	-10.6785	-3.58485	1.517481
C	-7.22519	-0.11486	-1.24161	H	-9.03528	-4.24692	1.531174
C	-9.34208	-5.8E-05	5.5E-05	H	-9.37921	-2.69955	2.338853
C	-10.0215	1.231796	-0.07678	H	-9.3008	-2.90602	-2.00487
C	-11.4246	1.206179	-0.07425	H	-8.99376	-4.37154	-1.04302
C	-12.1216	-0.00027	-7.2E-05	H	-10.6334	-3.70744	-1.15042
C	-11.4244	-1.20661	0.07416	H	-8.21001	2.362872	-0.16591
C	-10.0213	-1.23202	0.076813	H	-9.03583	4.246757	-1.53127
O	-7.87961	-0.21438	-2.30148	H	-9.37942	2.699267	-2.33887
O	-7.87958	0.214399	2.301589	H	-10.6789	3.584402	-1.51769
C	-9.28567	-2.56808	0.156296	H	-8.99453	4.37156	1.042927
C	-9.61595	-3.31867	1.466982	H	-9.30146	2.906056	2.004851
C	-9.57165	-3.44035	-1.08827	H	-10.6341	3.707222	1.150208
C	-9.28605	2.567973	-0.1563	H	3.152105	-0.33835	-3.37885
C	-9.61635	3.318406	-1.46707	H	5.611097	-0.3357	-3.33753
C	-9.57229	3.440288	1.088185	H	5.611144	0.335854	3.337468
C	2.903634	-0.12327	-1.24246	H	3.152152	0.338552	3.378818
C	3.605941	0.000107	-2E-05	H	11.97357	-2.13169	0.236435
C	2.90365	0.123495	1.242429	H	13.20707	-0.00048	1.91E-05
C	3.650771	-0.24247	-2.42338	H	11.97404	2.130998	-0.23641
C	5.050018	-0.2426	-2.41495	H	8.209248	-2.35499	0.251949
C	5.750476	-0.12279	-1.22108	H	9.02404	-4.43891	-0.79379
C	5.038239	9.55E-05	-2.9E-05	H	9.3571	-3.04442	-1.84733
C	5.750492	0.122957	1.221016	H	10.66623	-3.78312	-0.90523
C	5.050052	0.242775	2.41489	H	9.004955	-4.13845	1.766353
C	3.650804	0.242671	2.423341	H	9.322476	-2.53602	2.472007
C	7.225199	-0.12488	-1.24075	H	10.64588	-3.46946	1.747451
N	7.883554	4.79E-05	-4.3E-05	H	8.209788	2.355172	-0.25198
C	7.225217	0.125014	1.240662	H	9.005968	4.138506	-1.76624
C	9.341975	-7.3E-05	-2.7E-05	H	10.64674	3.469151	-1.74731
C	10.0211	-1.22696	0.135545	H	9.323162	2.536034	-2.47197
C	11.42421	-1.20161	0.133121	H	9.025072	4.438829	0.793924
C	12.12142	-0.00037	6.49E-06	H	10.66709	3.782589	0.905389
C	11.42447	1.201032	-0.13312	H	9.35772	3.044182	1.847392

References

[S1] Regar, R.; Mehra, K. S.; Bhowal, R.; Sankar, J. Electronic Modulation of Terrylene Diimides Leading to Core-Twisting, Tunable Emission and Intermolecular Interactions. *European J Org Chem* **2019**, *2019* (36), 6278–6284.

[S2] Chernowsky, C. P.; Chmiel, A. F.; Wickens, Z. K. Electrochemical Activation of Diverse Conventional Photoredox Catalysts Induces Potent Photoreductant Activity. *Angew. Chem., Int. Ed.* **2021,** *60* (39), 21418–21425.

[S3] Tomizaki, K. Y.; Thamyongkit, P.; Loewe, R. S.; Lindsey, J. S. Practical Synthesis of Perylene-Monoimide Building Blocks That Possess Features Appropriate for Use in Porphyrin-Based Light-Harvesting Arrays. *Tetrahedron* **2003**, *59* (8), 1191–1207.

[S4] Tong, L. H.; Pengo, P.; Clegg, W.; Lowe, J. P.; Raithby, P. R.; Sanders, J. K. M.; Pascu, S. I. Complexes of aryl-substituted porphyrins and naphthalenediimide (NDI): investigations by synchrotron X-ray diffraction and NMR spectroscopy. *Dalton Trans.* **2011**, 40(41), 10833–10842.

[S5] Aksakal, N. E.; Chumakov, Y.; Yuksel, F. Crystal Structures of Two Perylenediimides: A Study of Bay-Substitution. *J. Chem. Crystallogr*. **2019**, 49(2), 72–79.

[S6] Zhang, B.; Soleimaninejad, H.; Jones, D. J.; White, J. M.; Ghiggino, K. P.; Smith, T. A.; Wong, W. W. H. Highly Fluorescent Molecularly Insulated Perylene Diimides: Effect of Concentration on Photophysical Properties. *Chem. Mater.* **2017**, *29* (19), 8395–8403.

[S7] Y.S. Guan, A. Thukral, S. Zhang, K. Sim, X. Wang, Y. Zhang, F. Ershad, Z. Rao, F. Pan, P. Wang, J. Xiao, C. Yu,Air/water interfacial assembled rubbery semiconducting nanofilm for fully rubbery integrated electronics. *Sci. Adv.* **2020**, 6, eabb3656.

[S8] G. N. Jang, S. Y. Hong, H. Park, Y. H. Lee, H. Park, H. Lee, Y. R. Jeong, S. W. Jin, K. Keum, J. S. Ha,Highly sensitive pressure and temperature sensors fabricated with poly(3-hexylthiophene-2,5-diyl)-coated elastic carbon foam for bio-signal monitoring. *Chem. Eng. J.* **2021**, 423, 130197.

[S9] M. L. Singla, S. Awasthi, A. Srivastava, D. V. S. Jain, Effect of doping of organic and inorganic acids on polyaniline/Mn_3O_4 composite for NTC and conductivity behaviour. *Sens. Actuators, A.* **2007**, 136, 604–612.

[S10] A. Kumar, M. L. Singla, A. Kumar, J. K. Rajput,POMANI–Mn3O4 based thin film NTC thermistor and its linearization for overheating protection sensor. *Mater. Chem. Phys.* **2015**, 156, 150–162.

[S11] T. Jan, M. A. Rizvi, S. K. Moosvi, M. H. Najar, S. H. Mir, G. M. Peerzada,A Switching-Type Positive Temperature Coefficient Behavior Exhibited by PPy/(PhSe)2 Nanocomposite Prepared by Chemical Oxidative Polymerization. *ACS Omega.* **2021**, 6, 7413–7421.

[S12] X. Ren, P. K. L. Chan, J. Lu, B. Huang, D. C. W. Leung,High Dynamic Range Organic Temperature Sensor. *Adv. Mater.* **2013**, 25, 1291–1295.

[S13] M. Zhu, J. Cao, X. Wei, Y. He, A. Li, X. Xu, M. U. Ali, L. Yan, H. Meng,Self-supported hysteresis-free flexible organic thermal transistor based on commercial graphite paper. *Appl. Phys. Lett.* **2018**, 112, 253301.

[S14] N. Wu, Y. Zhang, C. Wang, P. M. Slattum, X. Yang, L. Zang,Thermoactivated Electrical Conductivity in Perylene Diimide Nanofiber Materials. *J. Phys. Chem. Lett.* **2017**, 8, 292–298.

[S15] J. Liu, X. Zhang, J. Zhang, S. Zhang, Y. Chen, H. Chen, H. Chen, M. Lin,Interpenetration of Donor–Acceptor Hybrid Frameworks for Highly Sensitive Thermal Sensors. *ACS Appl. Mater.* **2022**, 14, 24575–24582.

[S16] Frisch, M. J.; Trucks, G. W.; Schlegel, H. B.; Scuseria, G. E.; Robb, M. A.; **et al.** *Gaussian 16, Revision C.01*; Gaussian, Inc.: Wallingford, CT, **2016**.